Flight Flutter Test and Data Analysis Techniques Applied to a Drone Aircraft

Robert M. Bennett* and Irving Abel*
NASA Langley Research Center, Hampton, Va.

Modal identification results are presented that were obtained from recent flight flutter tests of a drone vehicle with a research wing called the DAST ARW-1 (for drones for aerodynamic and structural testing, aeroelastic research wing-1). This vehicle is equipped with an active flutter suppression system (FSS). Frequency and damping of several modes are determined by a time-domain modal analysis of the impulse response function obtained by Fourier transformations of data from fast-swept sine wave excitation by the FSS control surfaces on the wing. Flutter points are determined for two different altitudes with the FSS off. Data are given for near the flutter boundary with the FSS on.

Nomenclature

a_0	= coefficient in curve fit, the offset or static value [Eq. (1)]
a_k	= coefficient of kth cosine term in curve fit [Eq. (1)]
a_z	= acceleration, g
b_k	= coefficient of kth sine term in curve fit [Eq. (1)]
E	= mean-squared error [Eq. (2)]
$\hat{E}$	= expected value [Eq. (3)]
F	= Fourier transform
f	= frequency, Hz
h	= altitude, km (ft)
i	= data point index, 1-N
j	= parameter index
K	= number of modes in curve fit
k	= modal index, 1-K
M	= Mach number
N	= number of data points in digitized time history
R_l	= output error covariance matrix
$\hat{S}$	= parameter sensitivity matrix
t	= time, s
V	= velocity
V_f	= flutter velocity
Y	= curve-fitting expression [Eq. (1)]
Δp	= increment in parameter vector
δ	= control deflection, deg
ζ	= fraction of critical damping
η	= damping coefficient [Eq. (1)]
ω	= frequency, rad/s

Subscripts

l	= left wing
r	= right wing
c	= command signal

I. Introduction

ONE application of active controls technology to aircraft design is to suppress flutter. The potential benefits have been well demonstrated in wind-tunnel tests and by analysis (e.g., Refs. 1 and 2). A flight test program has been initiated by NASA to demonstrate active control technology including flutter suppression systems (FSS) in flight using a remotely piloted vehicle or drone aircraft. Free-flight data can thus be acquired on an aircraft with reduced risk. This program is called Drones for Aerodynamic and Structural Testing (DAST) and is a cooperative effort by the NASA Langley and Dryden Research Centers with contractual support from the Boeing Military Airplane Company, Wichita, Kansas. An overview of the DAST program is given in Ref. 3.

Three flights have been flown with the first aeroelastic research wing (ARW-1) from October 1979 to June 1980. Owing to several system problems including a hydraulic pump failure and difficulties with the telemetry systems, the first flight (October 1979) was essentially a systems development test. During the second flight (March 1980) sufficient structural dynamic response measurements were made with the flutter suppression system off (FSS off) to obtain a good estimate of the flutter Mach number for one altitude. The third flight (June 1980) included flutter testing with the FSS on and off. During this flight, flutter was encountered with the FSS on primarily as a result of an erroneous setting of the FSS gain to one-half the desired value. An overall description of these tests and on-line testing procedures, a description of the flutter incident, and some of the results of these flights are presented in Ref. 4.

The flight time of the DAST vehicle is limited to about 20 min. This short flight time and the additional complication of testing with the FSS both on and off required the development of a rapid testing technique. Fast-swept sine wave excitation by the FSS controls is used at each flight condition to yield data to define the dynamic characteristics of the vehicle. These dynamic data were analyzed on-line in near real time to determine the damping and frequency of the principal mode.[4] Subsequent data analysis has been performed after each flight to define additional modes. This paper presents the results of these post-test or off-line analyses of the fast-swept sine data using fast Fourier transform techniques along with a time-domain modal analysis[5] to extract the modal frequencies and dampings. A brief description of the overall test procedure is also presented and the modal analysis procedure is described. Flutter calculations for the DAST vehicle are compared in Ref. 6 with the experimental results of this paper.
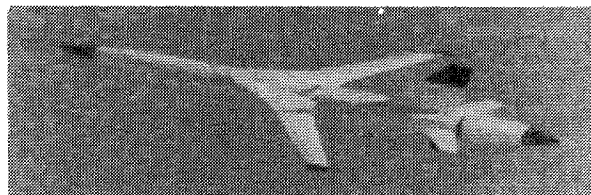
Fig. 1 DAST ARW-1 vehicle in flight.
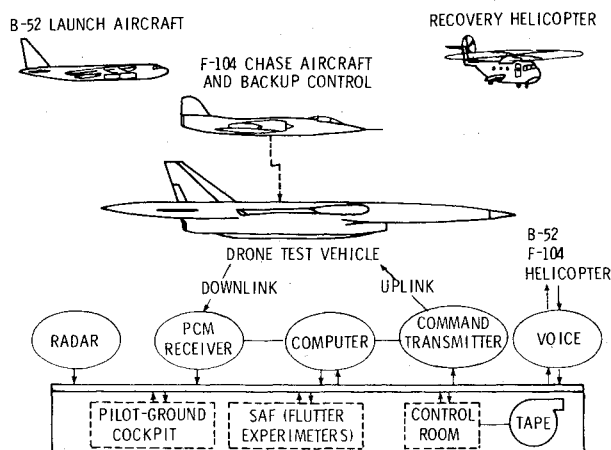
Fig. 2 DAST operational concept.
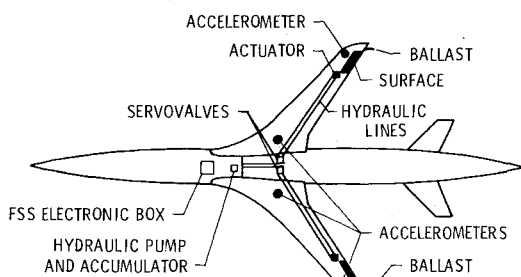
Fig. 3 Sketch of flutter suppression system, control surfaces, and sensor locations.

Fig. 4 Block diagram of post-test data analysis procedure.

II. Description of Vehicle and Tests

The DAST ARW-1 aircraft, shown in Fig. 1, is a modified Firebee II drone. It has an overall length of 8.6 m (28.3 ft). The ARW-1 research wing was designed for cruise near $M = 0.98$ and has a span of 4.34 m (14.3 ft), a supercritical airfoil section, and an aspect ratio of 6.8. The wing was designed to flutter within the flight envelope in order to assess the effectiveness of the onboard active control system used to suppress flutter.

The DAST operational concept is shown schematically in Fig. 2. The drone is carried aloft underneath the wing of a B-52, air launched, and flown remotely by a pilot in a ground cockpit. After a flight of 20-30 min, the drone is recovered by midair capture and retrieval by helicopter (Refs. 3 and 4 give further description of the operational aspects).

The DAST vehicle is extensively instrumented for measurement of rigid-body-type parameters, loads by calibrated wing strain-gage bridges, wing steady-state surface pressures, and the flutter system parameters. The data are digitized onboard and transmitted by two telemetry systems in pulse code modulated form to the ground for on-line use and recording. The sampling rate of the various channels varies from 20 to 500 samples per second (sps). Antialiasing filters were incorporated onboard for each channel. The high sample rate signals (500 sps) are used for the flutter system parameters and include the FSS accelerometers, the control position potentiometers, and the control system excitation signal. These data are recorded and later converted to a digital tape for computational analyses.

A sketch of the flutter suppression system for the DAST ARW-1 is shown in Fig. 3. The FSS includes wing tip and inboard accelerometers, a hydraulic control system with fast response actuators, wing aileron control surfaces, and onboard electronics. The FSS ailerons are used for flutter suppression and dynamic excitation but are not used for flight control of the aircraft. The system is designed to suppress
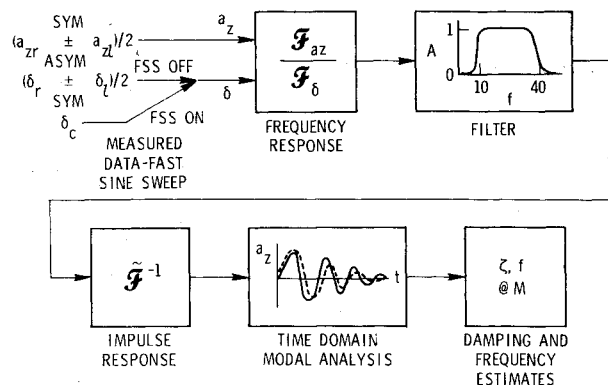
both symmetric and antisymmetric flutter and can be remotely engaged or disengaged by ground command in the structural analysis facility (SAF), where the flutter experimenters are located (Fig. 2). Since the flutter frequencies are in the 10-20 Hz range, the FSS control system is designed to respond at high frequencies. The lowest natural frequency for the control surface, actuator, and hydraulic system combination is near 50 Hz. This fast response aileron control system is also used for structural dynamic excitation. Control surface pulses (a single cycle of a 20-Hz sine wave) are used for qualitative on-line monitoring of aeroelastic stability, particularly during accelerating flight. For a more complete evaluation of stability, a fast-swept sine wave input by the controls is used. The swept sine signal runs from 10 to 40 Hz in 7 s and is tapered near the ends of the sweep to minimize transients, as suggested in Ref. 7. The sweeps of 7-s duration are considerably shorter than normally used in the flutter testing of aircraft. The short flight duration in combination with the need for symmetric, antisymmetric, FSS-on, and FSS-off testing led to the selection of the short duration of the sweeps. The relative high flutter frequency of 10-20 Hz also suggests that the sweep duration could be shorter than usually used for lower frequency modes. The sweeps and pulses are generated onboard the aircraft and are commanded from the ground by an operator in the SAF. Both symmetric and antisymmetric inputs can be generated. For test points of nominally constant flight conditions, a series of symmetric and antisymmetric sweeps and pulses are used. The data from the sweeps are analyzed on-line in near real time to obtain an indication of flutter mode stability.[4] For points below the predicted flutter boundary, the excitation is performed with the FSS both on and off. After the FSS-off flutter boundary is approached or exceeded, the FSS is left on and the testing is performed only for the system-on condition.

III. Data Analysis

Overall Procedure

The block diagram of the post-test analysis of the data with fast-swept sine wave inputs is presented in Fig. 4. The objective is to obtain good estimates of the frequency and damping of the modes of motion from the measured input and output signals. The procedure used here involves taking Fourier transforms of these signals numerically, forming the frequency response functions by dividing the transforms, and after a filtering operation, taking the inverse Fourier transform to obtain the impulse response function. The impulse response function contains the free vibration characteristics of the modes that respond to the excitation. A time-domain modal analysis procedure suitable for analysis of free vibration motion[5] is used to determine the frequency and damping of the principal modes. There are several alternative methods available for modal analysis (e.g., Refs. 5, 10, and 11), depending upon the type of data (frequency domain, etc.)

available and the desired form of the results. The method used is one that was designed for this type of data[5] and is conceptually simple. The data analysis procedure (Fig. 4) was implemented on the CDC CYBER 175 computers at Langley Research Center. The steps in this procedure are discussed in further detail in the following paragraphs.

The first step in the procedure is to sum the output of the left and right FSS accelerometers to minimize any extraneous antisymmetric motions occurring during symmetric excitation (Fig. 4) and to difference the accelerometer signals for antisymmetric excitation (as recommended in Ref. 8). The input signal for analyzing the data for FSS-off cases consists of the control deflection signals also summed or differenced depending on whether the motion is symmetric or antisymmetric. With the FSS on, the control deflection includes the sum of deflections in response to the excitation command and the deflections for flutter suppression. Use of the control deflection as the reference input signal gives the system off dynamics. For analysis with the FSS on, the sweep excitation command signal is used as the reference input signal (Fig. 4).

The discrete finite Fourier transforms of the input signal and the output signal (accelerometers) are calculated and the frequency response function is formed as the ratio of the two transforms. As previously indicated, the swept sine wave input ran from 10 to 40 Hz. Although the frequency response function is calculated from 0 to 250 Hz (the Nyquist frequency), there is essentially no input power and the frequency response function is meaningless outside the 10-40-Hz frequency range. Hence the frequency response function is filtered by multiplying by a window function in the frequency domain. The window function used is unity from 10 to 37.5 Hz, and is tapered with a $1 - \cos^2$ function from 7.5 to 10 Hz and from 37.5 to 42.5 Hz, and is zero at all other frequencies. The impulse response function is generated by taking the inverse Fourier transform of the filtered frequency response function. The filter function eliminates both spurious frequency response function estimates where the input power is nearly zero and any real noise or data in the frequency ranges where the filter function is zero. One consequence of band-limiting the frequency response function in this manner is a smearing of the impulse response function. The resulting impulse response function is a circular convolution of the transform of the filter function and the true impulse response function. This effect primarily produces a smearing phase error near the $t = 0$ portion of the impulse response. The 1-$\cos^2$ tapering decreases the side lobes of the time domain window, thus reducing the smearing effect. This tapering was chosen to be a compromise between noise elimination and windowing effects. The windowing effect is also partially alleviated by analyzing the impulse response starting at $t = 0.05$ (instead of $t = 0$) and by allowing additional terms in the complex exponential time-domain fitting technique. Generally a moderate amplitude term near the lower cutoff frequency (8-9 Hz) appears in the results and a small amplitude term near 40 Hz is occasionally obtained.

A similar data analysis procedure was used on-line for analyzing the fast-swept sine wave data with a minicomputer.[4] The on-line modal analysis assumed a single-degree-of-freedom model due to the time constraints of the flight, whereas the procedure used here takes into account all the principal modes in the response.

Modal Analysis Technique

The time-domain modal analysis procedure analyzes a single channel of data. Given a free decay record such as the impulse response function which contains the response of one or more vibration modes in the form of a digitized time history, the problem is to determine the damping, frequency, amplitude, and phase of each mode. A least-squares curve fit of the data is made with complex exponential functions (or

damped sine and cosine waves) in the form

$$Y(t) = a_0 + \sum_{k=1}^{K} e^{-\eta_k t} (a_k \cos \omega_k t + b_k \sin \omega_k t) \qquad (1)$$

The parameters a_0, a_k, b_k, η_k, and ω_k are determined such that the squared-error difference between the expression $Y(t_i)$ and measured time history a_z is minimized. The error is given by

$$E = \sum_{i=1}^{N} [Y(t_i) - a_{zi}]^2 \qquad (2)$$

Inspection of Eq. (1) shows that if η_k and ω_k and the value for K are known, it is possible to compute a_0, a_k, and b_k by solving a linear least-squares problem. The parameters η_k and ω_k enter the minimization problem in a nonlinear manner and must be determined by some type of search algorithm. Although this is a standard nonlinear optimization problem for which several methods are available, for simplicity, a direct search technique is used to search the coordinate space (η_k, ω_k) until a minimum is neared. A linearized technique is then used to accelerate convergence to the minimum. The method requires initial estimates for η_k and ω_k. For a single mode the initial estimates can be nearly arbitrary. However, for a multiple-mode case, the computer time can be significantly reduced by choosing good initial estimates. The following procedure has been found to be a reasonable way of getting the initial estimates for a multiple-mode case.

1) Generate a one-mode solution using arbitrary initial estimates.

2) Compute the difference between the one-mode solution and the input data, that is, the output error. Then generate a one-mode fit to the error.

3) Use the η_k and ω_k values from steps 1 and 2 as the initial estimates for the two-mode solution.

4) For higher modes, steps 2 and 3 are repeated using the difference between the current multimode solution and the original data to estimate the next higher mode. This procedure is continued until enough terms (K) are used to make the output errors small. This method has been implemented in a research code on the CDC CYBER 175. A typical run of a four-mode fit to 256 points in the time history takes about 50-60 s of CPU time including plotting.

Estimates of Standard Deviations of the Parameters

One difficulty with parameter estimation from dynamic data is determining the quality of the estimate. Usually, repeatability, scatter, etc., give the experimenter some indication of the quality of results. Another approach is to estimate the standard deviations of the determined parameters.[5] The standard deviations of the estimated parameters, or uncertainty levels, can be determined from maximum-likelihood theory (e.g., Ref. 12) based on the Cramer-Rao bound. This type of estimate has provided some useful results in the field of stability and control (e.g., Ref. 9). Assuming only measurement noise that is Gaussian and white, the expected variance of the parameter vector is

$$\hat{E}[\Delta p \Delta p^T] = \left\{ \sum_{i=1}^{N} \left[\hat{S}^T(t_i) R_I^{-1} \hat{S}(t_i) \right] \right\}^{-1} \qquad (3)$$

where $\hat{S}$ is the parameter sensitivity matrix, R_I is the output error covariance matrix (here a constant), and T denotes matrix transpose. The parameter vector p is made up of a_0, a_k, b_k, η_k, and ω_k. The parameter sensitivities are given by $S_j(t_i) = \partial Y(t_i) / \partial p_j$ and can be calculated by directly differentiating Eq. (1). The variance R_I is a normal output parameter of the program. Thus, for a single channel of data, as considered here, these parameter uncertainty levels can be readily calculated after the curve-fitting process is completed.
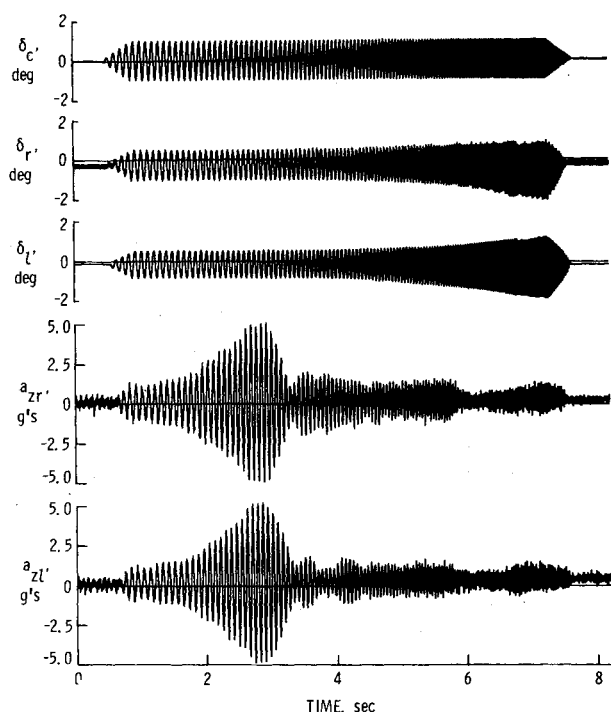
Fig. 5 Sample input control deflection and accelerometer responses for FSS off; $M = 0.74$, $h = 4.6$ km (15,000 ft).
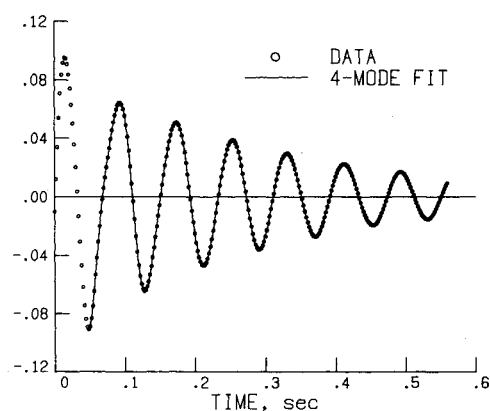

Fig. 6 Sample impulse response function and fit for FSS off; $M = 0.74$, $h = 4.6$ km (15,000 ft).
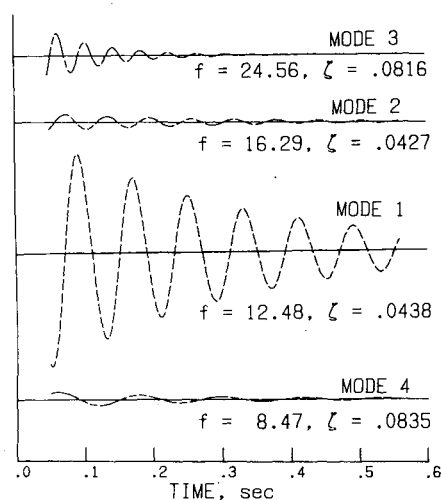

Fig. 7 Components of sample impulse response function for FSS off; $M = 0.74$, $h = 4.6$ km (15,000 ft).

Table 1 Normal mode frequencies predicted by NASTRAN analysis and measured during ground vibration test

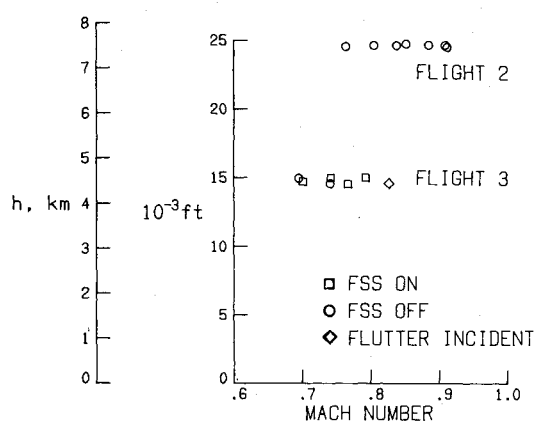| Mode	NASTRAN f, Hz	GVT f, Hz
Symmetric		
First wing bending	9.1	9.6
First fuselage bending	16.5	16.2
Wing bending torsion	29.6	29.1
	34.0	31.2
	39.8	40.6
	48.6	48.5
Antisymmetric		
First wing bending	12.3	13.5
First fuselage yaw	21.7	19.3
Wing bending torsion	30.0	27.0
	34.2	31.0
	36.0	...
	48.3	48.4

Fig. 8 Altitude and Mach number for test points.

One difficulty with the estimates of the standard deviations in the past has been that they gave unrealistically low values. This is discussed in Ref. 9 and is attributed to the fact that Eq. (3) assumes a uniform error spectrum, whereas in practice the error spectrum is band limited. In the present case the errors are largely a result of background modal response. Although some allowance for the actual spectrum of the error can be made, it is suggested[9] that multiplying the result calculated from Eq. (3) by 5-10 gives realistic results. A factor of 10 is used in this report. Experience has shown that these estimates are then a good qualitative guide to the validity of the estimated parameters.

Sample Case

An example of a time history recording from the DAST flight test is shown in Fig. 5. The response is from FSS off, symmetric excitation at $M = 0.74$, and $h = 4.6$ km (15,000 ft). The resulting impulse response function and a four-mode fit is shown in Fig. 6, and the modal content of the fit is shown in Fig. 7. The low-frequency mode labeled mode 4 is a result of the window function, as previously discussed, and is not a structural vibration mode. The three modes are identifiable by comparing with the ground vibration modal frequencies of Table 1. The first symmetric wing bending is mode 1, a symmetric wing-fuselage mode is mode 2, and mode 3 is the first symmetric torsion mode. The noise level both in the measured data (Fig. 5) and in the impulse response (Fig. 6) is very low.
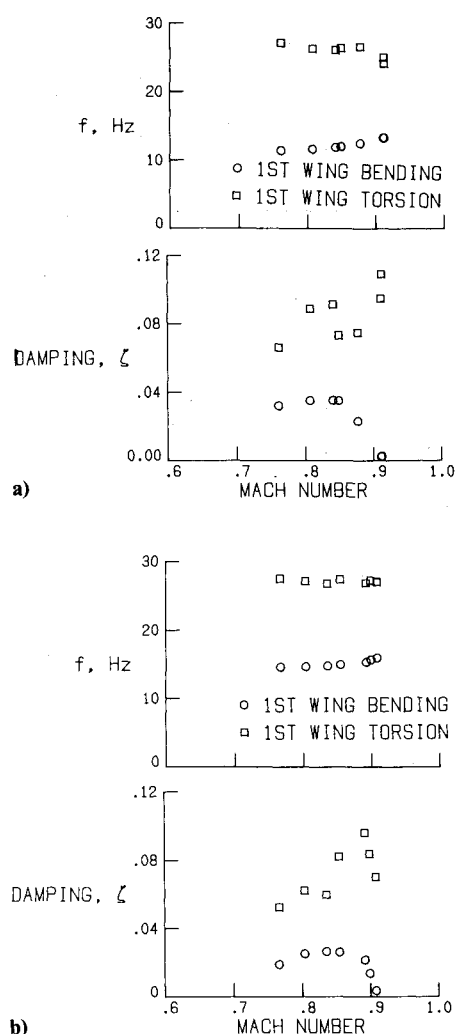
Fig. 9 Damping and frequency estimates for FSS off; 7.6 km (25,000 ft). a) Symmetric; b) antisymmetric.

Fig. 10 Standard deviations of frequency and damping estimates for FSS off; $h = 7.6$ km (25,000 ft). a) Symmetric; b) antisymmetric.

IV. Results and Discussion

Data from two flights showing the approach to the flutter boundary at two different altitudes will be discussed. The altitude and Mach number for the test points are shown in Fig. 8. The approach to near flutter for flight 2 was at a nominal altitude of 7.6 km (25,000 ft) with the FSS off. Both symmetric and antisymmetric data are presented for flight 2. For flight 3 the approach to flutter was for an altitude of approximately 4.6 km (15,000 ft). The data were taken with the FSS on and off at the lower Mach numbers, but only with the FSS on at the higher Mach numbers (Fig. 8). For flight 3, only data for the symmetric modes are presented, since they were critical for flutter with the FSS both on and off.

Tests at 7.6 km (25,000 ft) Altitude (Flight 2)

The estimated damping and frequency for the first bending and torsion modes for both symmetric and antisymmetric motion are shown in Fig. 9. The damping for the bending mode approaches zero and flutter is indicated near $M \approx 0.92$ for both symmetric and antisymmetric bending modes. There is little scatter apparent in the damping or frequency of the flutter mode and the flutter condition is approached with a moderate rate of decrease in damping with Mach number. The results for the torsion mode show some scatter, particularly in the damping values. The damping of the torsion mode increases and the frequency decreases as flutter is approached. These trends are typical for bending-torsion-type flutter as the flutter boundary is approached.
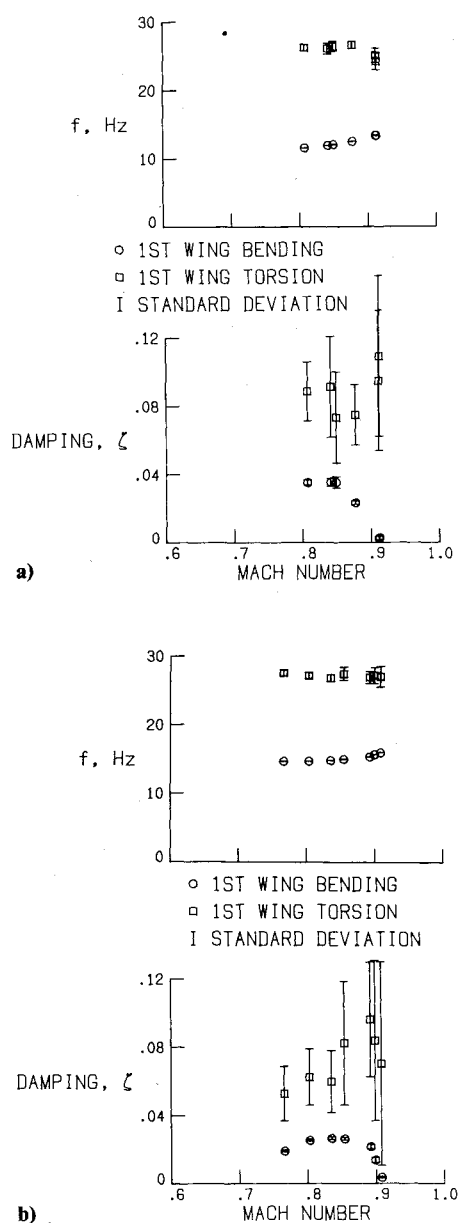
The data from Fig. 9 are repeated in Fig. 10 and the calculated standard deviations estimates are shown as the vertical bars through the symbols. The results indicate that the bending (flutter) mode is well estimated but that the torsional mode is not as well defined. This result is apparently a result of the higher damping and smaller amplitude of the torsion mode. The standard deviation estimates are consistent with the level of scatter and are smaller for the frequency than for damping. The result that frequencies are estimated more accurately than damping is generally the case for this type of data.

Four modes were used in fitting the impulse response function for these results. There is a fuselage first bending mode in the frequency range (Table 1), but it could not be reliably extracted from the FSS accelerometer data. Further definition might be possible from other data channels, such as the inboard accelerometers.

The results for the flutter mode indicate a low level of scatter and also correspond quite well to the on-line results.[5] This low level of scatter is likely a result of the low noise level in the data.
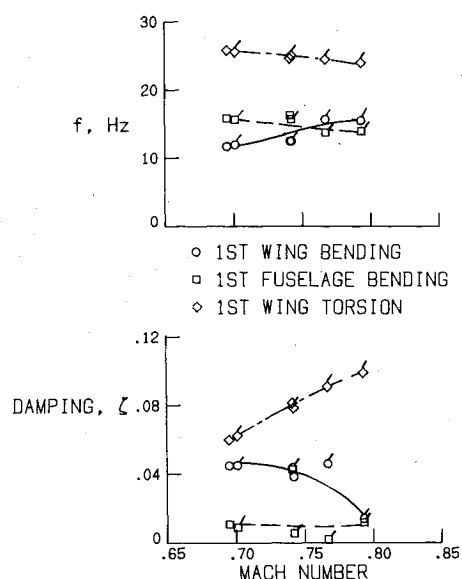
Fig. 11 Symmetric modal frequency and damping estimates for FSS off; $h = 4.6$ km (15,000 ft). Flagged symbols are FSS-off results calculated from FSS-on data.

## Tests at 4.6 km (15,000 ft) Altitude (Flight 3)

FSS Off

The symmetric damping and frequency estimates deter-mined for the FSS off are shown in Fig. 11. Three modes are indicated which correspond to the first wing bending, first fuselage bending, and first torsion. Flutter near $M = 0.80$ is indicated in the mode associated with the first symmetric wing bending. For this altitude there is a large interaction of the bending and fuselage modes and their frequencies apparently cross as Mach number is increased (Fig. 11). Dynamic data with response in two or more modes of nearly the same frequency can be troublesome for obtaining good estimates of the modal parameters. The trends shown by the lines in Fig. 11 are based primarily on continuity of the damping values and are possibly subject to some interpretation. These results were obtained using a four-mode approximation and the FSS accelerometer data.

The standard deviation estimates are shown in Fig. 12 for each of the three modes. The parameters are generally well estimated except for Mach numbers near 0.77, where the frequencies are nearly coincident. The fuselage modal par-ticipation was apparently sufficiently large at this altitude that the damping and frequency could be estimated. The damping for the fuselage mode is low and the standard deviation would indicate the possibility of instability. This mode was certainly stable for the FSS-off condition at $M = 0.70$ and $M = 0.74$, and the actual value of damping is more likely that of the symbols.

For the two Mach numbers for which measurements were made with the FSS both off and on, $M = 0.7$ and 0.74, the results for the FSS off are in very good agreement (Fig. 11). This good agreement also probably results from the low noise level in the measured data.

FSS On

The symmetric damping and frequency values determined for two of the principal modes with the FSS on are shown in Fig. 13. These two modes correspond to wing first bending and first torsion. The frequency of the bending mode is significantly raised by the FSS from 12-15 Hz to near 20 Hz. The damping is also significantly increased over that measured with the FSS off at the lower Mach numbers, but flutter would be projected to occur near $M = 0.80$ for the gain setting of the feedback system actually used for this flight.
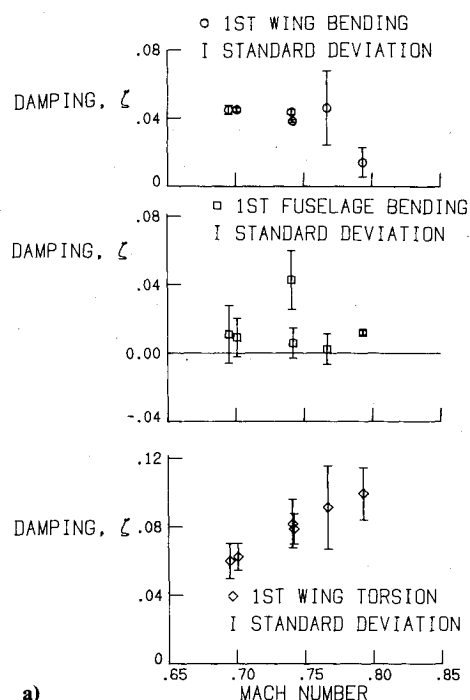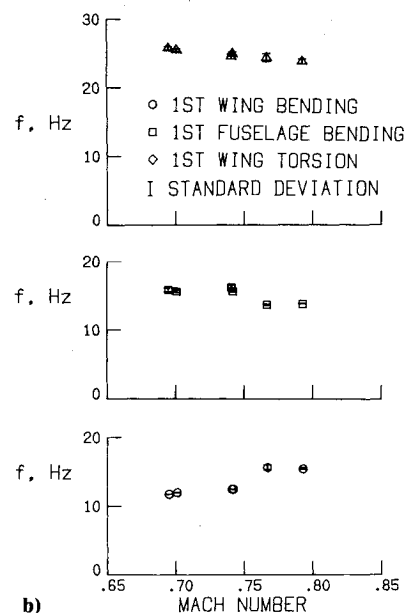
Fig. 12 Standard deviations of frequency and damping estimates for FSS off; $h = 4.6$ km (15,000 ft). a) Damping; b) frequency.

The aircraft was accelerating when the onset of sustained oscillation was obtained near $M = 0.817$. It had further ac-celerated to $M = 0.827$ when the divergent oscillations led to breakup of the right wing. The on-line damping estimates did not indicate the rapid onset of flutter, as shown in Fig. 13. Further discussion of the flutter incident is given in Ref. 4 and comparisons with analytical results are given in Ref. 6.

The estimates of the standard deviations of the damping and frequency values are shown in Fig. 14. The values for the bending mode are well determined except for the point at $M = 0.70$, which has a large standard deviation, possibly as a result of the higher damping value. The results for these two modes were determined from an eight-mode fit to the data, and are the two modes that were consistently determined from the response.
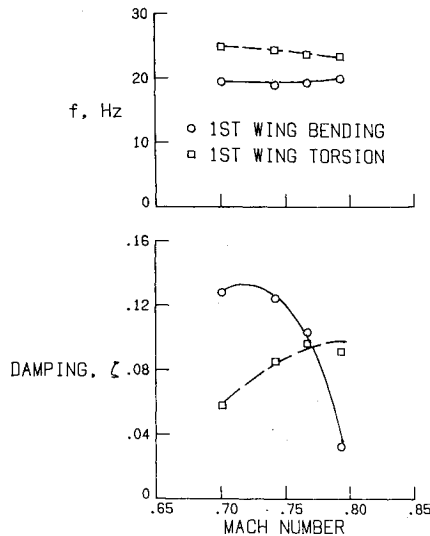
Fig. 13 Symmetric modal frequency and damping estimates for FSS on; $h = 4.6$ km (15,000 ft).
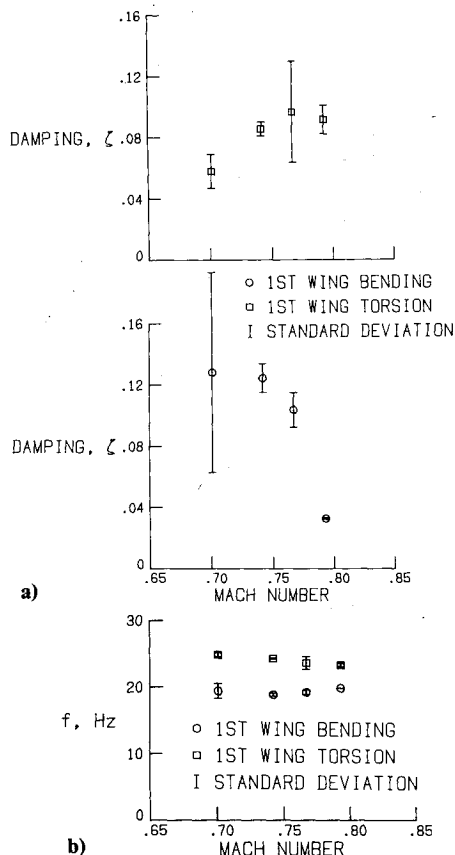

Fig. 14 Standard deviations of frequency and damping estimates for FSS on; $h = 4.6$ km (15,000 ft). a) Damping; b) frequency.

V. Concluding Remarks

The results of off-line analysis of data from two flights of the DAST ARW-1 have been presented. The dynamic characteristics of several modes have been obtained using the data analysis technique. This technique consisted of fast-swept sine excitation by the aileron controls and time-domain analysis of the impulse response function derived by numerical Fourier transform techniques. The approach to the flutter boundary is clearly defined by the results of this technique. A significant contributing factor in the success of this technique is the low level of noise in the measured data. The calculated standard deviation of the parameters based on the Cramer-Rao bound gives a useful qualitative indication of the quality of the frequency and damping estimates.

References

[1] Sandford, M.C., Abel, I., and Gray, D.L., "Development and Demonstration for Flutter Suppression System Using Active Controls," NASA TR R-450, 1975.

[2] "Report on a Cooperative Program on Active Flutter Suppression," AGARD Rept. 689, Aug. 1980.

[3] Murrow, H.N. and Eckstrom, C.V., "Drones for Aerodynamic and Structural Testing (DST), A Status Report," *Journal of Aircraft*, Vol. 16, Aug. 1979, pp. 521-526.

[4] Edwards, J.W., "Flight Test Results for an Active Flutter Suppression System Installed on a Remotely Piloted Vehicle," AIAA Paper 81-0655, April 1981.

[5] Bennett, R.M. and Desmarais, R.N., "Curve Fitting of Aeroelastic Transient Response Data with Exponential Functions," NASA SP-415, 1975, pp. 43-58.

[6] Newsom, J.R. and Pototzky, A.S., "Comparison of Analysis and Flight Test Data for a Drone Aircraft with Active Flutter Suppression," AIAA Paper 81-0640, April 1981.

[7] Jennings, W.P., Olsen, N.L., and Walter, M.J., "Transient Excitation and Data Processing Techniques Employing the Fast Fourier Transform for Aeroelastic Testing," NASA SP-415, 1975, pp. 77-115.

[8] Houbolt, J.C., "On Identifying Frequencies and Damping in Subcritical Flutter Testing," NASA SP-415, 1975, pp. 1-42.

[9] Maine, R.E. and Iliff, K.W., "Estimation of the Accuracy of Dynamic Flight-Determined Coefficients," AIAA Paper 80-171, 1980.

[10] Gaukroger, D.R., Skingle, C.W., and Heron, K.W., "Numerical Analysis of Vector Response Loci," *Journal of Sound and Vibration*, Vol. 29, No. 3, 1973, pp. 341-353.

[11] Ibrahim, S.R., "Modal Confidence Factor in Vibration Testing," *The Shock and Vibration Bulletin*, Bull. 48, Part 1, Sept. 1978, pp. 65-75.

[12] Grove, R.D., Bowles, R.L., and Mayhew, S.C., "A Procedure for Estimating Stability and Control Parameters from Flight Test Data by Using Maximum Likelihood Methods Employing a Real-Time Digital System," NASA TN D-6735, 1972.